Preparation of mesocarbon microbeads by thermal polymerization of the blended coal tar and biomass tar pitch as anode material for sodium-ion batteries

Lei Li, Jie Liu, Xiaochen Liu, Wanyue Wu[*]

School of Chemical Engineering, Sichuan University of Science and Engineering, Sichuan, Zigong 643000, PR China
[*]E-mail: lilei20150620@yeah.net

Sodium ion batteries (SIBs) are capable of low redox potential, low cost and stable electrochemical performance and thus have attracted increasing attentions, while the defects of smaller theoretical specific capacity and the difficulty in ion insertion or ion extraction restrict their further improvements. To solve this problem, soft carbon anode materials such as mesocarbon microbeads (MCMBs) severed as anode were developed. In this work, Mesocarbon microbeads (MCMBs) were prepared from coal tar pitch (CTP) in the presence of biomass tar pitch (BTP) by heating-treatment from ambient temperature to 410 $^{\circ}$C for 7 h. XRD analysis indicates that graphite-like crystallites the carbonized MCMBs with an interlayer distance of 0.345-0.351 nm. Interlayer distance of carbonized MCMBs prepared from CTP is 0.336 nm. Raman analysis indicates carbonized MCMBs prepared with BTP possess more defect sites than those from CTP. MCMB anode prepared by CTP and BTP exhibits higher charge and discharge capacity, keeping a charge capacity of 236.6 mA h g^{-1} with the capacity retention rate 94.7% after 70 cycles. Co-carbonization of BTP and CTP are capable of enlarging the degree of cross-linking of MCMBs and form a relatively stable cross-linked structure inside, the layer spacing and microcrystalline structure of MCMBs is beneficial to the insertion/extraction of sodium ion. Sodium intercalation into graphene layers is the dominant step regarding sodium storage mechanism in MCMBs

1. INTRODUCTION

Development of Lithium-ion batteries (LIBs) has attracted great research interests due to its' high energy capacity with broad application prospects [1]. However, the issue of insufficient distribution of lithium resources causes high cost for mineral exploitation and shortage [2, 3]. To tackle this issue, sodium-ion batteries (SIBs) is subsequently developed in response to high demand of low-priced battery

[4-6]. According to current research progress [7-10], SIBs are capable of low-cost, lower redox potential (-2.71 V vs standard hydrogen electrode for Na^+/Na versus -3.04 V for Li^+/Li) and stable electrochemical performance when compared with LIBs [11]. While larger atomic radius of sodium atom (70% than lithium atom) leads to smaller theoretical specific capacity than lithium (1/2 of lithium) and the difficulty in ion insertion or ion extraction. The drawback of SIBs may inevitably create an obstacle regarding substitution of LIBs with SIBs [12].

In recent years, a significant number of research on anode materials for SIBs has been reported and majority of them is mainly focused on investigation of carbons and non graphitable carbons [13-17]. Hard carbon material has irregular grain orientation and large interlayer spacing that enables sodium intercalate/deintercalate in expanded graphite with an enlarged interlayer spacing of ~ 0.43 nm [18], with high reversible capacities of 200-300 mA h g^{-1}. However, practical applications of hard carbon as anode electrode material used in SIBs is rarely reported. The main reason is that the capacities rapidly fade during cycling and sodium metal deposited in the porous carbon material is difficult to be desorborbed [1]. Although some soft carbon materials also have been studied for SIBs, to have high safety and the sodium storage capacity comes from the intercalation of sodium, the soft carbon materials show low reversible capacities and poor cycle performance during charge and discharge [19-21].

As a soft carbon material, mesocarbon microbeads (MCMBs) have been widely used in anode materials of LIBs [22-24], applications in SIBs are also reported [25-27]. MCMBs has unique layered structure of organic aromatic hydrocarbons and mesophase pitch nucleus, so it is easy to form graphite-like layered structures after being carbonized. Their surface layer is mainly disordered and dense, which can prevent the decomposition of carbon crystallites during frequent discharge/charge cycling, the interlayer spacing and defect sites of MCMBs are the main factors affecting the performance of ion batteries [2, 28].

In this paper, MCMBs were prepared from coal tar pitch (CTP) in the presence of biomass tar pitch (BTP) by heating-treatment, BTP can increase the interlayer spacing and defect sites of MCMBs. Their electrochemical performance as potential anode for SIBs was investigated and discussed in detail.

2. EXPERIMENTAL

2.1. Material

In this study, the CTP as the preliminary feedstock was provided by a coke production company, China, the contents of C, H and O element in CTP are 92.32, 4.42 and 1.473 wt.%. BTP was provided by a biomass tar production company, China, the contents of C, H and O element in BTP are 60.49, 7.33 and 31.49 wt.%, BTP has higher oxygen content and higher H/C atom ratio compared with CTP.

2.2. Preparation of MCMBs

The green MCMBs were prepared from BTP-CTP mixtures in a stainless-steel autoclave, and the autoclave was heated from ambient temperature to 410 ℃ for 7 h under a nitrogen atmosphere. The MCMBs after separation and carbonization were labeled as MCMB-0, MCMB -10, MCMB -15 and MCMB -20, where 0, 10, 15 and 20 represent the proportion of BTP added in BTP-CTP mixtures.

2.3. Preparation of electrodes

Using MCMBs as the negative electrode material, the carbonized MCMBs, PVDF and acetonitrile were mixed at a mass ratio of 8: 1: 1 in a certain amount of NMP, and stirred for 30 min to form a slurry. The slurry was pasted on copper foil, after the coated copper foil was dried and was pressed, punched into a diameter of about 13 mm disks serves as the anode electrodes. Using sodium sheet with a size of Φ17 mm×0.5 mm for the counter electrode. The battery separator was polypropylene microporous film (Cellgard 2400), and the electrolyte is 1 M $NaPF_6$/EC+DEC. The battery assembly was operated in a glove box with argon as protective gas.

2.4. Characterizations

The constant current charge and discharge performance of the prepared button ion battery was tested with a LAND tester (LAND CT2001A, China). The charge and discharge voltage range were 0~2.5V. The MCMB ion battery was subjected to constant current density at 10, 20, 50, 100, 500, 1000 and 1500 mA g^{-1}. the cyclic voltammetry characteristics of the battery electrodes was performed on an electrochemical workstation (A CHI660D, CHInstruments, China), the voltage scan range is 0~2.5V, and the scan speed is 0.1 mV s^{-1}.

3. RESULTS AND DISCUSSION

3.1. Morphologies and structural characteristics of MCMB

As a follow-up to a previous study [29], our research team conducted a more detailed study on the structural characteristics of carbonized MCMBs samples. Of the two investigated samples, MCMB-15 was found to have the higher yield, the smaller average particle size and larger layer spacing. XRD and Raman results showed that layers of MCMBs prepared by thermal polymerization of CTP blended with BTP are mainly disordered and compact and can thus prevent the decomposition of carbon crystallites during frequent discharge/charge cycling [2]. The high interlayer spacing of MCMB-15 promotes insertion/extraction of ions and thus facilitates ion storage. Therefore, MCMB-15 is selected as the most suitable raw material for preparing battery anode.

3.2 Electrochemical characteristics of the materials
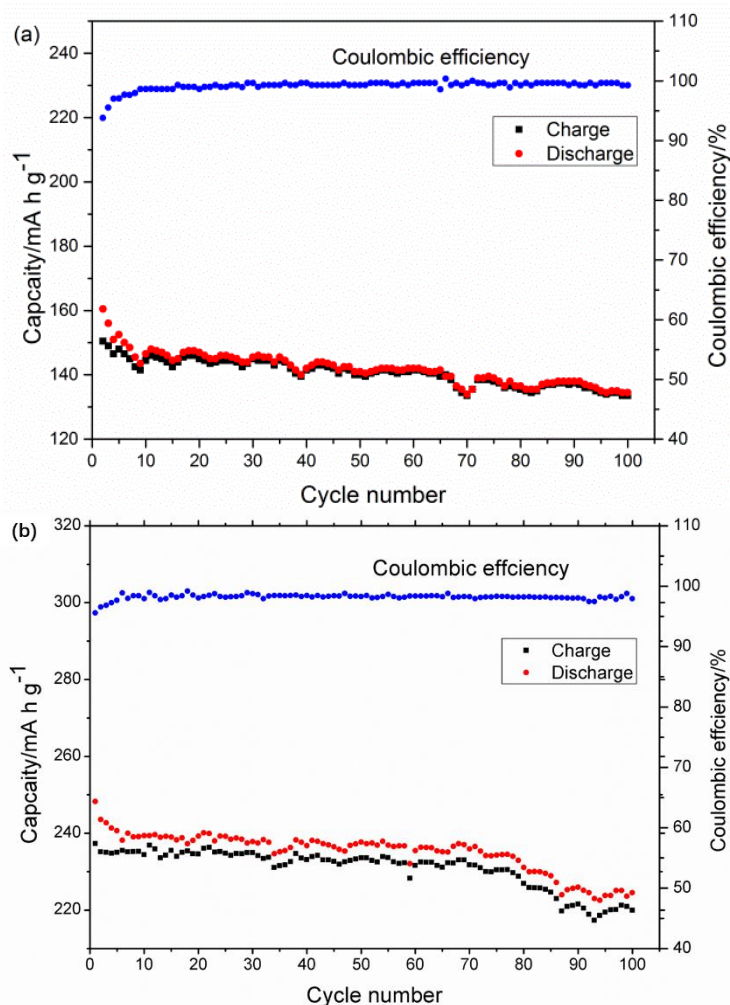
Figure 1. Cyclic performance of MCMB-0 (a) and MCMB-15 (b) materials used in sodium-ion batteries at a current density of 20 mA g^{-1}.

Fig.1 shows the charge-discharge cycle performance curves of MCMB-0 and MCMB-15 used as anode electrodes of SIBs under a current density of 20 mA g^{-1}. The first-charge capacities of MCMB-0 and MCMB-15 are 160.5 and 237.3 mA h g^{-1}, respectively. After 100 charge-discharge cycle tests, the reversible sodium storage specific capacities of MCMB-0 and MCMB-15 are 134.5 and 219.9 mA h g^{-1}, respectively. The capacity retention rates of the MCMB-0 and MCMB-15 are 88.0% and 92.7%, and the charge capacity and capacity retention rate of MCMB-15 are higher than those of MCMB-0. **Fig. 1** (a) shows that the first coulombic efficiency and last cycle efficiency of MCMB-0 are 93.8% and 98.5%, respectively. **Fig. 1** (b) shows that the first coulombic efficiency and last cycle efficiency of MCMB-15 are 95.6% and 98.9%, respectively. Both samples maintain good coulombic efficiency after multiple cycles. Both samples maintain good coulombic efficiency after multiple cycles. MCMB-15 has higher sodium storage capacity and structural stability during cycling than MCMB-0 mainly because of the relatively stable cross-linked structure formed in the MCMB upon addition of BTP. The higher coulombic efficiency of MCMB-15 than MCMB-0 also indicates that the structure of MCMB-15 is more

favorable for the insertion and extraction of sodium, even though this structure is not particularly stable during the early stage of charging and discharging. Sodium loss during electrolyte decomposition and SEI formation affect the first coulombic efficiency [31].
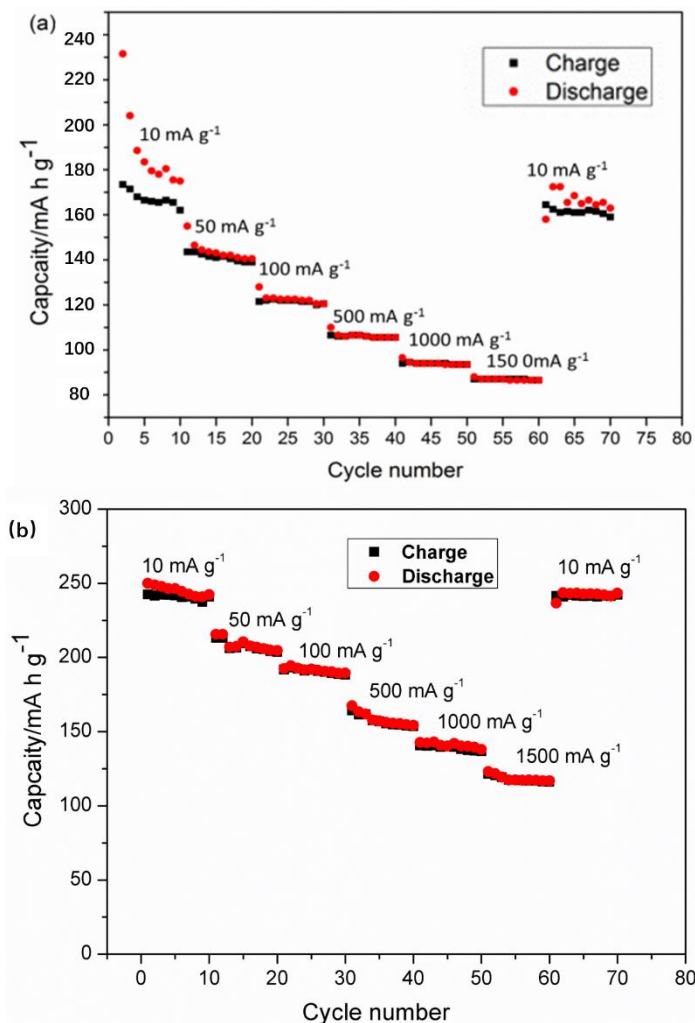
Figure 2. Rate performance of MCMB-0 (a) and MCMB-15 (b) at a current density between 10 and 1500 mA g^{-1}

Fig. 2 shows the results of rate performance tests on MCMB-0 and MCMB-15. Fig. 2(b) clearly shows that over a range of test current densities of 10 mA g^{-1} to 1500 mA g^{-1}, MCMB-15 has a considerably higher charge specific capacity than MCMB-0 at a high current density. The reversible specific capacity of MCMB-15 at each current density are 242.4, 207.4, 191.8, 164.2, 140.6 and 121.4 mA g^{-1}, and the reversible sodium storage capacity retention of MCMB-15 can reach 50.1%, even at 1500 mA g^{-1}. **Fig.2**(a) shows that the reversible specific capacities of MCMB-0 are 174.3, 145.6, 122.3, 108.6, 92.8 and 84.3 mA g^{-1} at various current densities from 10 mA g^{-1} to 1500 mA g^{-1}, respectively. The capacity retention rate of MCMB-0 is 48.4% at high current density of 1500 mA g^{-1}.

These results indicate that the MCMB-15 electrode has a higher rate performance than MCMB-

0 because the addition of BTP changes the structure of MCMBs, which increases the interlayer spacing of microcrystalline carbon and the defect sites to facilitate the reversible storage and transmission of sodium in the material even at high rates.
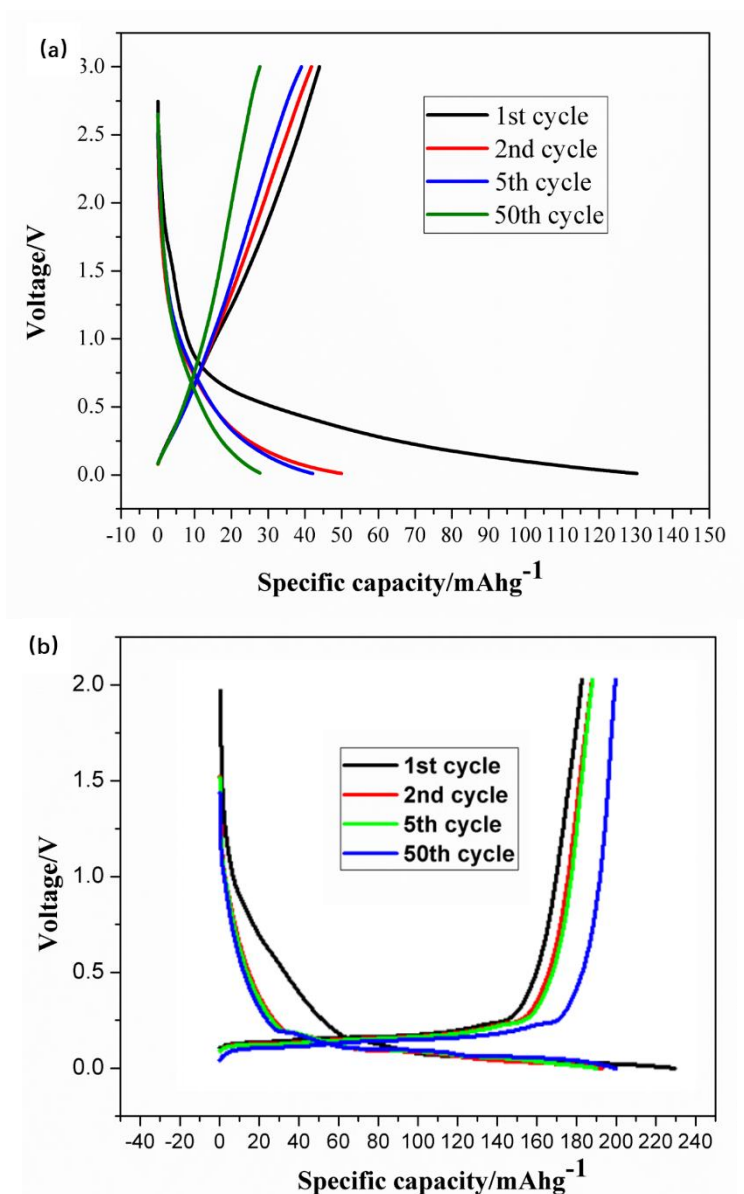
Figure 3. Discharge-charge curves of the MCMB-0 (a) and MCMB-15 (b) in density of 25 mA g^{-1}

A constant current charge-discharge test of the half-cell was carried out at a current density of 25 mA g^{-1}. **Fig. 3** shows that the discharge curve of MCMB-0 and MCMB-15 electrode decrease rapidly from open circuit voltage to approximately 1 V and then gradually decrease from 1 to 0 V and plateau. This low-potential plateau corresponds to the voltage range over which sodium is stored, that is, sodium

ions are first embedded into the defect sites of the carbon layer on MCMB surface. With decreasing discharge voltage, sodium ions are embedded further into the graphite-like microcrystalline carbon layers in the MCMB. Compared to MCMB-15 curve, the MCMB-0 curve is shorter and steeper, indicating that MCMB-0 has a lower capacity than MCMB-15. The main reason for this result is that MCMB-15 contains more defect sites and larger internal microcrystalline carbon layers spacing than MCMB-0.

Fig. 3(a) shows that the initial discharge/charge specific capacity and coulombic efficiency for MCMB-0 are 130.3/43.7 mA h g^{-1} and 33.7%, respectively. The high irreversible capacity of the first cycle is mainly due to SEI film formation, which consumes a portion of the sodium. The other discharge/charge curves have a similar profile.
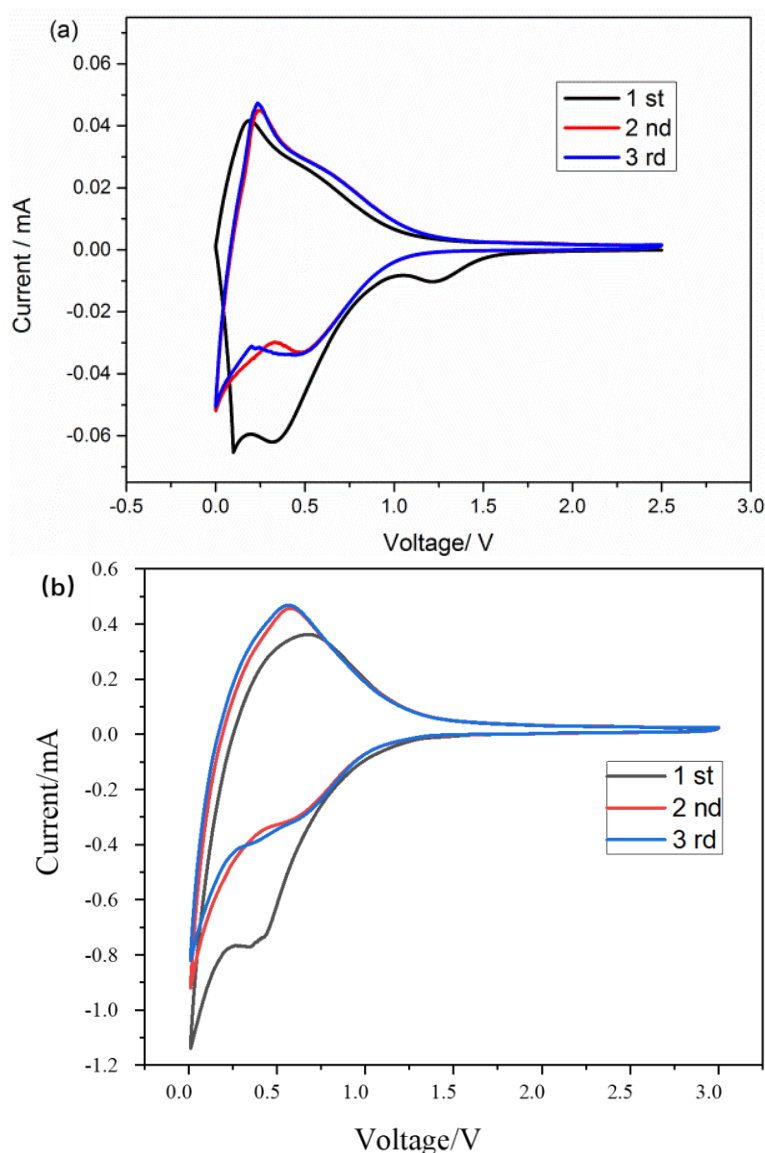
Figure 4. CV curves in the initial three cycles of MCMB-0 (a), MCMB-15 (b) measured in a voltage window between 0 and 3 V at a scan rate of 0.1 mV s^{-1}

Fig.3(b) presents a low coulombic efficiency (79.6%) during the first charge-discharge cycle,

which also results from the formation of SEI layers, However, the SEI film protects the anode material, preventing the material from collapsing or being destroyed and increasing its cycle life. The other discharge/charge curves show similar monotonic profiles with no discernible plateaus, which is consistent with the curve of soft carbon [32].

The electrochemical behavior of MCMB-0 and MCMB-15 is further characterized based on the cyclic voltammetry (CV) results obtained at a slow scan rate (0.1 mV s^{-1}), as shown in **Fig. 4**. The reduction peak area of MCMB-0 and MCMB-15 for the first cycle is significantly larger than the oxidation peak area, and the loss of capacitance is mainly caused by SEI film formation or electrolyte decomposition [33]. MCMB-0 and MCMB-15 show similar profiles after the first cycle, indicating that both materials have stable electrochemical properties. **Fig. 4**(a) shows that the reduction peak at 0-0.2 V, which corresponds to the insertion of sodium ions into the carbon microspheres, and an oxidation peak at approximately 0.25 V, which corresponds to the extraction of sodium ions from the carbon microspheres. **Fig. 4**(b) shows that the reduction peak at 0-0.2 V, which corresponds to the insertion of sodium ions into the carbon microspheres, and an oxidation peak at approximately 0.5 V, which corresponds to the extraction of sodium ions from the carbon microspheres (based on reports in the literature [34, 35]). Comparing the cyclic voltammetry curves of MCMB-0 with MCMB-15 electrodes under the same voltage conditions shows that the MCMB-0 electrode has a smaller current than the MCMB-15 electrode. This result shows that MCMB-0 has a lower capacity than MCMB-15.

The high oxygen concentration in BTP, results in the formation of oxygen-containing functional groups during the pyrolysis process with CTP [36]. The oxygen-containing functional group can accelerate the crosslink and condensation reaction. That is, co-carbonization of BTP and CTP can increase the degree of cross-linking of MCMBs to produce a relatively stable cross-linked structure thereby freezing the movement of pitch molecules in the subsequent carbonization process. The resulting change in the layer spacing and microcrystalline structure of MCMBs promotes ion transport and charge transfer. The addition of BTP can increase the number of defect sites in the carbon microspheres, which promotes storage of sodium ions in the material.

Table 1. The charge specific capacity and ICE data of samples

Sample	Charge capacity /50mAh g^{-1}	ICE/%(The first discharge/charge at 25 mA g^{-1})	ICE/%(samples after 100 cycles at 100 mA g^{-1})
MCMB-15	223	79.6	92.7
C-MCMB700 [28]	186	63.3	77.2
OC-MCMB360 [28]	222	62.6	83.0

Table 1 summarizes the charge specific capacity and ICE data of samples. OC-MCMB360 represents a sample of MCMB after air oxidation at 360 °C and carbonization，C-MCMB700 is a low temperature carbonized MCMB sample without oxidation treatment [28]. The Table shows that both addition of BTP and air oxidation can improve the electrochemical performance of MCMBs as anodes for sodium-ion batterie. The ICE of MCMB-15 after the first discharge/charge at 25 mA g^{-1} and 100 cycles at 100 mA g^{-1} is slightly better than that of OC-MCMB360. This indicates that both air oxidation

and BTP addition can change the structure of MCMBs. In addition to increases the interlayer spacing of microcrystalline carbon and the defect sites appropriately through cross-linking reactions, the high hydrogen content in BTP reduces the viscosity of the carbonization system, which is also beneficial to change the structure of MCMB.

4. CONCLUSIONS

In this work, MCMBs were successfully prepared as anode material for sodium-ion batteries by thermal polymerization of CTP with blending of BTP. Carbonized MCMBs were also prepared with BTP possess larger interlayer spacing and more defect sites than those from CTP alone. Compared with MCMB anode prepared by CTP, MCMB anode prepared by CTP and BTP exhibit higher charge and discharge capacity, and keep a charge capacity of 261.9 mA h g^{-1} and the capacity retention rate 99.1% after 70 cycles. Co-carbonization of BTP and CTP can increase the degree of cross-linking of MCMBs and produce a relatively stable cross-linked structure inside, the layer spacing and microcrystalline structure of MCMBs, which promotes storage of sodium ions in the material. Sodium intercalation into graphene layers being the dominant sodium storage mechanism in MCMBs.

References

1. L. J. Song, S. S. Liu, B. J. Yu, C. Y. Wang, M. W. Li, *Carbon,* 95(2015)972. https://doi.org/10.1016/j.carbon.2015.09.032
2. J. X. Wang, Y. P. Zhang, Y. Guo, M. W. Li, C.Y. Wang. *Ionics,* 27(2021)677-682. https://doi.org/10.1007/s11581-020-03835-8
3. N. Yabuuchi, K. Kubota, M. Dahbi, S. Komaba, *Chem. Rev*, 114(2014)11636. https://doi.org/10.1021/cr500192f
4. S. Janakiraman, M. Khalifa, R. Biswal, S. Ghosh, S. Anandhan, A. Venimadhav, *J. Power Sources*, 460(2020)1. https://doi.org/10.1016/j.jpowsour.2020.228060
5. M. W. Lu, Y. Huang, C. Chen, *Energy & Fuels*, 34(2020)11489. https://doi.org/10.1021/acs.energyfuels.0c01841
6. P. Du, L. Cao, B. Zhang, C. Wang; Z. M. Xiao, *Renew Sust Energ Rev*, 151(2021)1. https://doi.org/10.1016/j.rser.2021.111640
7. L. P. Wang, L. H. Yu, X. Wang. *J. Mater. Chem* A, 3(2015)9353. https://doi.org/10.1039/C4TA06467D
8. B. Cao, H. Liu. B. Xu, Y. F. Lei, X. H. Chen, H. H. Song, *J. Mater. ChemA,* 4(2016) 6472. https://doi.org/10.1039/C6TA00950F
9. J. Y. Hwang, S. T. Myung, Y. K. Sun, *Chem Soc Rev*, 46(2017)3529. https://doi.org/10.1039/C6CS00776G
10. H. L. Pan, Y. S. Hu and L. Q. Chen, *Energy Environ Sci*, 6(2013)2338. https://doi.org/10.1039/c3ee40847g
11. C. Bommier, W. Luo, W. Y. Gao. A, Greaney; S. Q. Ma, X. L. Ji. *Carbon,* 76(2014)165.

https://doi.org/10.1016/j.carbon.2014.04.064
12. Y. Li, Y. Lu, P, Adelhelm, M. M. Titirici, Y. S. Hu, *Chem Soc Rev*, 48(2019) 4655.
    https://doi.org/10.1039/C9CS00162J
13. R. Alcántara, J. M. Jiménez-Mateos, P. Lavela, J. L. Tirado, *Electrochem Commun*, 3(2001)639.
    https://doi.org/10.1016/S1388-2481(01)00244-2
14. P. Thomas, D. Billaud, *Electrochim Acta*, 47(2003)3303.
    https://doi.org/10.1016/S0013-4686(02)00250-5
15. J, Jin, B. J. Yu, Z. Q. Shi, C. Y. Wang, C. B. Chong, *J Power Sources*, 272(2014)800.
    https://doi.org/10.1016/j.jpowsour.2014.08.119
16. L. Y. Pei, L. T. Yang, H. L. Cao, P. Z. Liu, M. Zhao, *Electrochim Acta*, 364(2020)137313.
    https://doi.org/10.1016/j.electacta.2020.137313
17. J. Jin, Z. Q. Shi, C. Y. Wang, *Electrochim Acta*, 141(2014)302.
    https://doi.org/10.1016/j.electacta.2014.07.079
18. Y. Wang, Y. Yang, L. Yan, S. Y. Kwork, W. Li, *Nat. Commun*, 5(2014)4033/1.
    https://doi.org/10.1038/ncomms5466
19. K. Tang, R. J. White, X. K. Mu, M. M. Titirici, P. A. van Aken, J. Maier, *Chemsuschem*, 5(2012)400-403.
    https://doi.org/10.1002/cssc.201100609
20. A. Suryawanshi, D. Mhamane, S. Nagane, S. Patil, V. Aravindan, *Electrochim Acta*, 146(2014)21.
    https://doi.org/10.1016/j.electacta.2014.09.052
21. Y, Matsuo, K, Ueda, *J Power Sources*, 263(2014)158.
    https://doi.org/10.1016/j.jpowsour.2014.04.038
22. M. D. Fang, T. H. Ho, J. P. Yen, Y. R. Lin, J. L. Hong, *Materials*, 8(2015)3550.
    https://doi.org/10.3390/ma8063550
23. J. Yao, G. X. Wang, J. H. Ahn, H. K. Liu, S. X. Dou, *J Power Sources*, 114(2003)292.
    https://doi.org/10.1016/S0378-7753(02)00585-2
24. H. Liu, Z. Shan, W. Huang, D. D. Wang, Z. J. Lin, *ACS Appl Mater Inter*, 10(2018)4715.
    https://doi.org/10.1021/acsami.7b16760
25. R. Alcántara, F. J. Fernández Madrigal, P. Lavela, J. L. Tirado, J. M. Jiménez Mateos, *Carbon*, 38(2000)1031.
    https://doi.org/10.1016/S0008-6223(99)00215-8
26. S. Sun, C. Y. Wang, M. Chen, M. W. Li, L. Wang, *J Colloid Interf Sci*, 426(2014)206.
    https://doi.org/10.1016/j.jcis.2014.04.012
27. D. Zhao, Q. Ru, S. Hu, X. H. Hou, *Ionics*, 23(2017)897.
    https://doi.org/10.1007/s11581-016-1884-x
28. C. Yuan, Y. Y. Zhu, P. Y. Zhao, B. J. Yu, Q. Li, C. Y. Wang, *ChemElectroChem*, 4(2017)2583.
    https://doi.org/10.1002/celc.201700529
29. L. Li, X. C. Lin, J. He, Y. K. Zhang, J. X. Lv, Y. G. Wang, *J Anal Appl Pyrol,* 155(2021)105039.
    https://doi.org/10.1016/j.jaap.2021.105039
30. A. Sadezky, H. Muckenhuber, H. Grothe, R. Niessner, U. Pöschl, *Carbon*, 43(2005)1731.
    https://doi.org/10.1016/j.carbon.2005.02.018
31. D. A. Stevens; J. R. Dahn, *J Electrochem Soc*, 148(2001)A803.
    https://doi.org/10.1149/1.1379565
32. Z. Jie, L. Zhao, N. Dimov, S. Okada, J. I. Yamaki, *Journal Power Sources*, 244(2013)752.
    https://doi.org/10.1016/j.jpowsour.2013.06.109
33. J. D. Zhu, C. Chen, Y. Lu, Y. Q. Ge, H. Jiang, *Carbon*, 94(2015)189.
    https://doi.org/10.1016/j.carbon.2015.06.076
34. K. Tang, L. Fu and R. J. White, L. H. Yu; M. M. Titirici, *Adv Energy Mater*, 2(2012)873.
    https://doi.org/10.1002/aenm.201100691
35. Z. Jiang, M. Alamgir, K. M. Abraham, *J Electrochem Soc*, 42(1995)333.

https://doi.org/10.1149/1.2043997
36. L. Li, X. Lin, Y. Zhang, J. Z. Dai, D. P. Xu, Y. G. Wang, *J Anal Appl Pyrol*, 150(2020)104889.
    https://doi.org/10.1016/j.jaap.2020.104889